BLIND IMAGE DEBLURRING IN THE EDGE DOMAIN

S. Colonnese, P. Campisi**, G. Panci*, G. Scarano**

*Dip. INFOCOM, Università "La Sapienza" di Roma
via Eudossiana 18, I-00184 Roma, Italy
Tel:+39.06.44585.500, Fax:+39.06.4873.300

**Dip. Elettronica Applicata, Università degli Studi "Roma Tre"
via Della Vasca Navale 84, I-00146 Roma, Italy
Tel:+39.06.5517.7064, Fax:+39.06.5517.7026

e-mail: (*)(gpanci,colonnese,scarano)@infocom.uniroma1.it
(**) campisi@uniroma3.it

ABSTRACT

This work addresses the problem of blind image deblurring, having one or more observations of the original image obtained through unknown linear channels and corrupted by additive noise. We resort to an iterative algorithm, belonging to the class of Bussgang algorithms, based on alternating a linear and a nonlinear image estimation stage. Specifically a novel nonlinear processing is performed on the Radon Transform of the image edges. The effect of the nonlinear processing is to thin the blurred image edges, and to drive the overall blind restoration algorithm to a focused image. The performance of the algorithm are assessed by experimental results pertaining to restoration of blurred natural images.

1. INTRODUCTION

The problem of blind image deblurring, that is of recovering an original image observed through one or more linear channels, has been recently addressed in a number of papers [1], [2]. Moreover, different approaches resort to suitable image representation domains. To cite a few, in [3] a wavelet based edge preserving regularization algorithm is presented, while in [4] the image restoration is accomplished using simulated annealing on a suitably restricted wavelet space. In [5] the authors make use of the Fourier phase for image restoration [6] applying appropriate constraints in the Radon domain.

In [7], the authors resort to an iterative algorithm, belonging to the class of Bussgang algorithms, based on alternating a linear and a nonlinear image estimation stage.

In this paper we investigate the design of the nonlinear processing stage using the Radon Transform (*RT*) [8] of the image edges. This choice is motivated by the fact that the *RT* of the image edges well describes the structural image features and the effect of blur, thus simplifying the nonlinearity design.

The herein discussed approach shares some common points with [9], since it exploits a compact multiscale representation of natural images.

2. OBSERVATION MODEL

The single-input multiple-output (SIMO) observation model of images is analytically characterized by:

$$y_i[m,n] = (x * h_i)[m,n] + v_i[m,n], \tag{1}$$

for $i = 0, \cdots, M-1$. The additive terms $v_i[m,n]$ represent realizations of mutually uncorrelated zero mean white Gaussian processes, statistically independent of the image $x[m,n]$.

The restored image $\hat{x}[m,n]$ is obtained from the observations $y_i[m,n]$ by means of a bank of M linear FIR restoration filters $f_i[m,n]$, $i = 0, \cdots, M-1$, whose support is $(2P+1 \times 2P+1)$, namely:

$$\hat{x}[m,n] = \sum_{i=0}^{M-1} \sum_{t,u=-P}^{P} f_i[t,u]\, y_i[m-t, n-u] \tag{2}$$

3. MULTICHANNEL BUSSGANG ALGORITHM

The scheme of the iterative multichannel Bussgang blind deconvolution algorithm, as presented in [7], is depicted in Fig. 1. The linear restoration stage is accomplished using a bank of FIR restoration filters $f_i^{(k)}[m,n]$, $i = 0, \cdots, M-1$, with finite support of size $(2P+1) \times (2P+1)$, namely

$$\begin{aligned} \hat{x}^{(k)}[m,n] &= \sum_{i=0}^{M-1} (y_i * f_i^{(k)})[m,n] \\ &= \sum_{i=0}^{M-1} \sum_{t,u=-P}^{P} f_i^{(k)}[t,u]\, y_i[m-t, n-u] \end{aligned} \tag{3}$$

At each iteration a nonlinear estimate $\tilde{x}^{(k)}[m,n] = \eta(\hat{x}^{(k)}[m,n])$ is then obtained from $\hat{x}^{(k)}[m,n]$. Then, the filter coefficients are updated by solving the following linear system (*normal equations*)

$$\sum_{j=0}^{M-1} \sum_{t,u=-P}^{P} R_{y_j y_i}[r-t, s-u] f_j^{(k)}[t,u] = R_{\tilde{x}^{(k-1)} y_i}[r,s]$$

for $i = 0, \cdots, M-1$ and $r, s = -P, \cdots, P$. As outlined in [11, 12], the iterative algorithm reaches an equilibrium point when

$$R_{\hat{x}^{(k)} y_i}[r,s] = \text{const} \cdot R_{\tilde{x}^{(k)} y_i}[r,s]. \tag{4}$$

4. BUSSGANG NONLINEARITY DESIGN USING THE RADON TRANSFORM IN THE EDGE DOMAIN

The quality of the restored image obtained by means of the Bussgang algorithm heavily depends on the capability of the adopted nonlinearity $\eta(\cdot)$ to restore specific characteristics of the original image.

If the unknown image is well characterized using a probabilistic description, as for text images, the nonlinearity $\eta(\cdot)$ can be designed on the basis of a Bayesian criterion, as the "best" estimate of $x[m,n]$ given $\hat{x}^{(k)}[m,n]$. Often, the Minimum Mean Square Error (MMSE) criterion is adopted. For natural images, we design the nonlinearity $\eta(\cdot)$ after having represented the linear estimate[1]

[1] To simplify the notation, in the following we will drop the superscript $^{(k)}$ referring to the k-th iteration of the deconvolution algorithm.

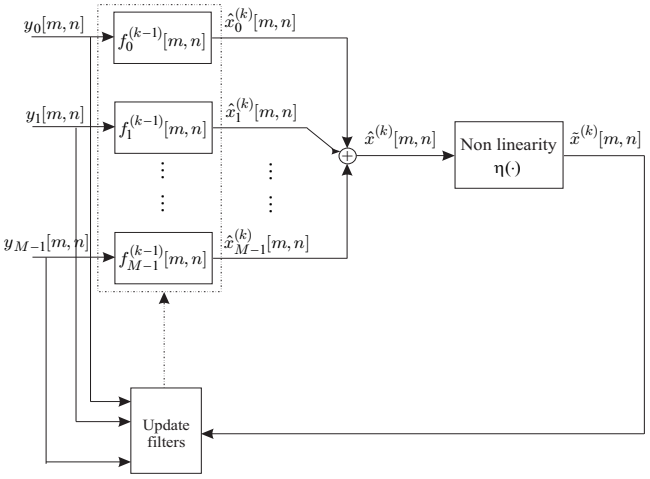

Figure 1: General form of the Bussgang deconvolution algorithm.

$\hat{x}[m,n]$ in a transformed domain in which both the blur effect and the original image structural characteristics are easily understood.

Let us consider the decomposition of the linear estimate $\hat{x}[m,n]$ by means of a filter pair composed by the lowpass filter $\psi^{(0)}[m,n]$ and a bandpass filters $\psi^{(1)}[m,n]$ (see Fig.2) whose impulse responses are

$$\begin{cases} \psi^{(0)}[m,n] = e^{-r^2[m,n]/\sigma_0^2} \\ \psi^{(1)}[m,n] = \dfrac{r[m,n]}{\sigma_1} e^{-r^2[m,n]/\sigma_1^2}\, e^{-j\theta[m,n]} \end{cases} \tag{5}$$

where $r[m,n] \stackrel{\text{def}}{=} \sqrt{m^2+n^2}$, and $\theta[m,n] \stackrel{\text{def}}{=} \arctan n/m$ are discrete polar pixel coordinates. These filters belong to the class of the Circular Harmonic Functions (CHF) [13], briefly summarized in Appendix A, and possess the interesting characteristic of being invertible by a suitable filter pair $\phi^{(0)}[m,n], \phi^{(1)}[m,n]$.

The zero-order circular harmonic filter $\psi^{(0)}[m,n]$ extracts a lowpass version $\hat{x}_0[m,n]$ of the input image. By choosing the form factor σ_0 small enough, in the pass-band the blur transfer function is approximately constant, and thus the blur effect on the lowpass component results negligible. The first order circular harmonic filter $\psi^{(1)}[m,n]$ is a bandpass filter, with frequency selectivity set by properly choosing the form factor σ_1. The output of this filter is a complex image $\hat{x}_1[m,n]$, which will be referred to in the following as "edge image", whose magnitude is related to the presence of edges and whose phase is proportional to their orientation. Therefore a local analysis of the edge image can yield a classification of each pixel as belonging either to edges or to textured regions or uniform ones.

We resort to the analyze the edges present in $\hat{x}_1[m,n]$ by means of the local application of the bidimensional *RT*.

This transform has the property to map a straight line in a point of the transformed domain, and therefore it yields a compact and meaningful representation of the image edges. Since most image edges are curves, this property applies only locally, that is on regions small enough such that the piece of the interested line appears straight. It is worth pointing out that our approach shares the digital *RT* as a tool used in a a family of recently proposed image transforms, the curvelet transforms [9], [10], which have the capability to provide a sparse representation of both smooth image functions and edges.

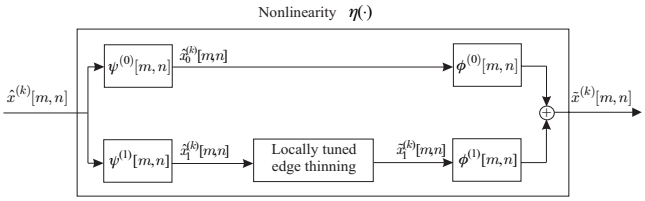

Figure 2: Multiresolution nonlinear estimator $\eta(\cdot)$.

4.1 Local Radon Transform of the Edge Image

For a continuous image $\xi(t_1,t_2)$ the *RT* is defined as

$$p_\beta^\xi(s) \stackrel{\text{def}}{=} \int_{-\infty}^{\infty} \xi\left(\cos\beta\cdot s - \sin\beta\cdot u,\ \sin\beta\cdot s + \cos\beta\cdot u\right)\, du,$$

with $-\infty < s < \infty$, $\beta \in [0,\pi)$. It is well known that it can be inverted by

$$\xi(t_1,t_2) = \frac{1}{4\pi^2}\int_0^\pi \int_{-\infty}^{\infty} P_\beta^\xi(j\sigma) e^{j\sigma(\sigma\cos\beta\, t_1 + \sigma\sin\beta\, t_2)} |\sigma|\, d\sigma d\beta$$

where $P_\beta^\xi(j\sigma) = \mathcal{F}\left\{p_\beta^\xi(s)\right\}$ is the Fourier transform of the *RT*.

If the image $\xi(t_1,t_2)$ is frequency limited in a circle of diameter D_Ω, it can be reconstructed by the samples of its *RT* taken at spatial sampling interval $\Delta s \le 2\pi/D_\Omega$,

$$p_\beta^\xi[n] = p_\beta^\xi(s)|_{s=n\cdot\Delta s} \quad n = 0, \pm1, \pm2, \cdots$$

Moreover, if the original image is approximately limited in the spatial domain, *i.e.* it vanishes out of a circle of diameter D_t, the sequence $p_\beta^\xi[n]$ has finite length $N = 1 + D_t/\Delta s$. In a similar way, the *RT* can be sampled with respect to the angular parameter β considering M different angles $m\Delta\beta$, $m = 0, \cdots, M-1$, with sampling interval $\Delta\beta$, namely

$$p_{\beta_m}^\xi[n] = p_{\beta_m}^\xi(s)|_{s=n\cdot\Delta s,\ \beta_m = m\cdot\Delta\beta}$$

The angular interval $\Delta\beta$ can be chosen so as to assure that the distance between points $p_\beta^\xi[n]$ and $p_{\beta+\Delta\beta}^\xi[n]$ lying on adjacent diameters remains less or equal than the chosen spatial sampling interval Δs, that is

$$\Delta\beta \cdot \frac{D_t}{2} \le \Delta s$$

The above condition is satisfied when $M \ge \frac{\pi}{2}\cdot N \simeq 1.57\cdot N$.

To summarize, under the hypothesis that the original image is approximately spatially bounded and bandwidth limited and that $N - 1 \ge D_t \cdot D_\Omega/2\pi$, and $M \ge \frac{\pi}{2}\cdot N$, the M, N samples

$$p_{\beta_m}^{x_1}[n], m = 0, \cdots M-1, n = 0, \cdots N-1$$

of the *RT* $p_\beta^{x_1}(s)$ allow the reconstruction of the image $\xi(t_1,t_2)$, and hence of any pixel of the selected region.

4.2 Nonlinearity Design in the Radon domain

The nonlinearity has to be designed according to the fact that each pixel can belong to different regions: strong edges, weak edges, and textured regions.

For significant image edges, characterized by relevant energy concentrated in one direction, the nonlinearity can exploit the spatial memory related to the edge structure. In this case, as above

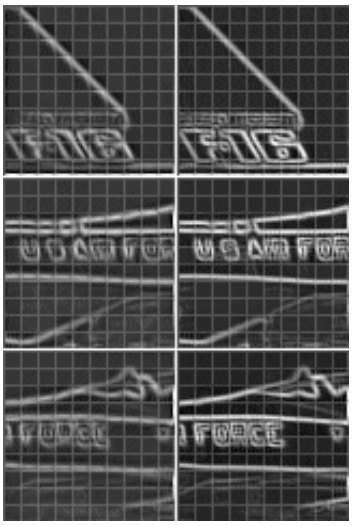

Figure 3: First column: details of a blurred test image in the edge domain. Second column: corresponding restored details in the edge domain.

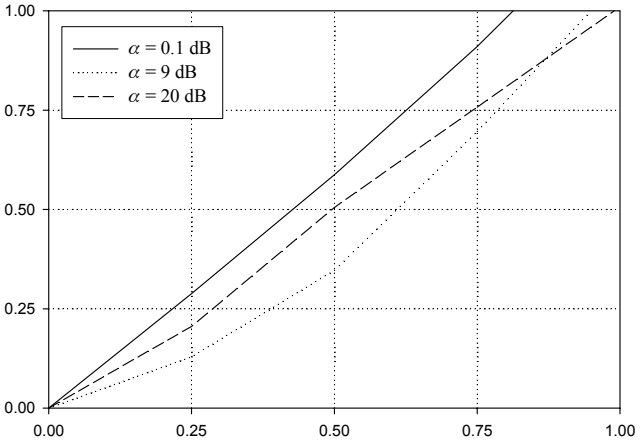

Figure 4: Nonlinearity given by (9), employed for natural images deblurring, parameterized with respect to the parameter α for $\gamma = 0.5$.

discussed, we use the Radon transform of the edge image. Let us consider a limited area of the edge image $\hat{x}_1[m,n]$ interested by an edge, and its *RT* $p^{\hat{x}_1}_{\beta_m}[m,n]$, with m,n chosen as discussed in 4.1. The nonlinearity we present aims at focusing the *RT* both with respect to m and n, and it is given by:

$$p^{\tilde{x}_1}_{\beta_m}[n] = p^{\hat{x}_1}_{\beta_m}[n] \cdot f^{\kappa_f}(n, \beta_m) \cdot g^{\kappa_g}(\beta_m) \tag{6}$$

where

$$f(n, \beta_m) = \frac{p^{\hat{x}_1}_{\beta_m}[n] - \min_n(p^{\hat{x}_1}_{\beta_m}[n])}{\max_n(p^{\hat{x}_1}_{\beta_m}[n]) - \min_n(p^{\hat{x}_1}_{\beta_m}[n])} \tag{7}$$

and

$$g(\beta_m) = \frac{\max_n(p^{\hat{x}_1}_{\beta_m}[n]) - \min_{\beta_k,n}(p^{\hat{x}_1}_{\beta_k}[n])}{\max_{\beta_k,n}(p^{\hat{x}_1}_{\beta_k}[n]) - \min_{\beta_k,n}(p^{\hat{x}_1}_{\beta_k}[n])} \tag{8}$$

For each point of direction β_m and index n, the nonlinearity (6) weights the *RT* by two gain functions. The first function depends on the distance between the actual value of the Radon transform $p^{\hat{x}_1}_{\beta_m}[n]$ and the maximum value competing to the same direction β_m. The second function depends on the distance between the maximum value competing to the same direction β_m and the global maximum.

To depict the effect of the nonlinearity (6) in the edge domain, in Fig.3 some details extracted from blurred versions of a test image are shown along with their corresponding restored counterpart in the edge domain. The edges result clearly enhanced and focused by the processing.

If the image is locally low contrast or does not exhibit any directional structure able to driven the nonlinearity, we use a spatially zero memory nonlinearity acting pointwise on the edge image. Since the edge image is almost zero in every pixel corresponding to the interior of uniform regions, where small values are likely due to noise, the nonlinearity should attenuate low magnitude values of $\hat{x}_1[m,n]$. On the other hand, high magnitude values of $\hat{x}_1[m,n]$, possibly due the presence of structures, should be enhanced. A pointwise nonlinearity performing the said operations is given in the following:

$$\begin{aligned} \tilde{x}_1[m,n] &= (1+1/\alpha) \cdot \hat{x}_1[m,n] \cdot g\left(\left|\hat{x}_1[m,n]\right|\right) \\ g(\cdot) &= 1 + \gamma \cdot \sqrt{1+\alpha} \cdot \exp\left[-\frac{(\cdot)^2}{2} \cdot \frac{\alpha}{(1+1/\alpha)}\right] \end{aligned} \tag{9}$$

The magnitude of (9) is plotted in Fig.4 for different values of the parameter α. The nonlinearity (9) has been presented in [7], where the analogy of this nonlinearity with the Bayesian estimator of spiky images in Gaussian observation noise is discussed.

After the nonlinear estimate $\tilde{x}_1[m,n]$ has been computed, the estimate $\tilde{x}[m,n]$ is obtained by reconstructing through the inverse filter-bank $\phi^{(0)}[m,n]$ and $\phi^{(1)}[m,n]$, *i.e.* (see Fig.2):

$$\tilde{x}[m,n] = \left(\phi^{(0)} * \hat{x}_0\right)[m,n] + \left(\phi^{(1)} * \tilde{x}_1\right)[m,n] \tag{10}$$

5. EXPERIMENTAL RESULTS AND CONCLUSIONS

The images used in our experimentations have been blurred using the blurring filters having the following impulse responses:

$$h_1[m,n] = \begin{bmatrix} 0 & 0 & 0 & 1 & 0 & 0 & 0 \\ 0 & 0 & 0 & 1 & 0 & 0 & 0 \\ 0 & 0 & 0 & 1 & 0 & 0 & 0 \\ 0 & 0 & 0 & 1 & 0 & 0 & 0 \\ 0 & 0 & 1 & 0 & 0 & 0 & 0 \end{bmatrix}; \quad h_2[m,n] = \begin{bmatrix} 0 & 0 & 0 & 1 & 0 & 0 & 0 \\ 0 & 0 & 0 & 1 & 0 & 0 & 0 \\ 0 & 0 & 0 & 1 & 0 & 0 & 0 \\ 0 & 0 & 1 & 0 & 0 & 0 & 0 \\ 0 & 0 & 1 & 0 & 0 & 0 & 0 \end{bmatrix};$$

$$h_3[m,n] = \begin{bmatrix} 0 & 0 & 0 & 0 & 0 & 0 & 0 \\ 0 & 0 & 0 & 0 & 0 & 0 & 0 \\ 0.5 & 0.86 & 0.95 & 1 & 0.95 & 0.86 & 0.5 \\ 0 & 0 & 0 & 0 & 0 & 0 & 0 \\ 0 & 0 & 0 & 0 & 0 & 0 & 0 \end{bmatrix}$$

In Fig.5 some details belonging to a test image are depicted. The corresponding blurred observations, affected by additive white Gaussian noise at SNR = 20dB, obtained using the aforementioned blurring filters are also shown as long as the deblurred images. In Fig.6 the MSE, defined as

$$\text{MSE} \stackrel{\text{def}}{=} \frac{1}{N^2} \sum_{i,j=0}^{N-1} \left(x[i,j] - \hat{x}[i,j]\right)^2$$

is plotted *vs.* the iteration number at different SNR values for the deblurred image.

It is worth noting that the deblurring algorithm furnishes images of improved visual quality, significantly reducing the distance, in the mean square sense, from the original unblurred image.

In summary an algorithm for blind image restoration that iteratively performs a linear and a nonlinear processing is here described. The nonlinear stage is based on a suitable nonlinear processing designed in the Radon transformed domain that leads to a sharp, focused image.

Figure 5: "F16" image. First column: details of the original image. Second, third, and fourth column: blurred observations of the original details. Fifth column: restored details. (SNR = 20 dB)

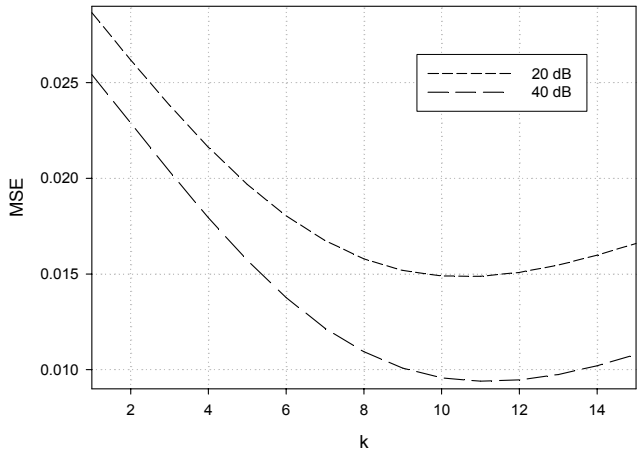

Figure 6: Mean Square Error versus the iteration number.

Appendix A. CIRCULAR HARMONIC FUNCTIONS

Referring to a continuous polar coordinate system, namely (r,θ), the functions

$$\psi^{(n)}(r,\theta) = \frac{w(r)}{2\pi r} e^{-jn\theta} \tag{A.1}$$

are known in literature as circular harmonic functions (CHFs) of order n with radial profile $h_n(r) \stackrel{\text{def}}{=} w(r)/2\pi r$. The zero-order CHF, obtained from (A.1) for $n = 0$, gives as output a real valued image which is a lowpass version of the input image. In general, the $n-th$ order CHF is tuned to the fundamental harmonics of n-fold angular symmetric patterns, corresponding to edges $(n = 1)$, lines $(n = 2)$, forks $(n = 3)$, crosses $(n = 4)$ and so on.

For the application carried out in this paper, we have considered a discrete implementation of the following polar separable continuous functions

$$\psi^{(n)}(r,\theta) = r^n e^{-r^2} e^{-jn\theta} \tag{A.2}$$

with $n = 0, 1, 2, 3, \cdots$, known as "marginal" Hermite filters.

REFERENCES

[1] G. Harikumar, Y. Bresler, "Perfect blind restoration of images blurred by multiple filters: theory and efficient algorithm", *IEEE Transactions on Image Processing*, Vol.8, pp.202-219, February 1999.

[2] G.B. Giannakis, R.W. Heath Jr., "Blind Identification of multichannel FIR Blurs and Perfect Image Restoration", *IEEE Transactions on Image Processing*, Vol.9, pp.1877-1896, November 2000.

[3] M. Belge, M.E. Kilmer, E.L. Miller, "Wavelet domain image restoration with adaptive edge-preserving regularization", *IEEE Transactions on Image Processing*, vol. 9, no. 4, pp.597-608, April 2000

[4] M.C. Robini, I.E. Magnin, "Stochastic nonlinear image restoration using the wavelet transform", *IEEE Trans. on Image Processing*, vol. 12, No. 8, August 2003

[5] D.P.K. Lun ,T.C. Hsung,T.W. Shen "Orthogonal discrete periodic Radon transform. Part II:applications", *Signal Processing*, vol. 83, No 5, May 2003.

[6] R.G. Lane, R.H.T. Bates, "Relevance for blind deconvolution of recovering Fourier magnitude from phase", *Opt. Commun.*, Vol. 63, July 1987.

[7] G. Panci, P. Campisi, S. Colonnese, G. Scarano "Multichannel blind image deconvolution using the Bussgang algorithm: spatial and multiresolution approaches", *IEEE Transactions on Image Processing*, vol.12, No.11, November 2003.

[8] S. R. Deans, **The Radon transform and some of its applications**, Krieger publishing company, 1993.

[9] J. Starck, E.J. Candes, D.L. Donoho "The curvelet transform for image denoising", *IEEE Transactions on Image Processing*, Vol.11, pp.678-684, June 2002.

[10] D. L. Donoho and M. R. Duncan, "Digital curvelet transform: Strategy, implementation and experiments," *SPIE Vol. 4056*, pp. 12-29, 2000.

[11] R. Godfrey, F. Rocca, "Zero memory nonlinear deconvolution", in *Geophysical Prospecting 29*, pp189-228, 1981.

[12] S. Bellini, "Bussgang techniques for blind deconvolution and restoration", in **Blind Deconvolution**, S. Haykin ed., Prentice-Hall, 1994.

[13] G. Jacovitti, A. Neri, "Multiresolution circular harmonic decomposition", *IEEE Trans.Signal Processing*, Vol. 48, pp. 3242-3247, November 2000.